



This is a repository copy of *Big GABA II: Water-referenced edited MR spectroscopy at 25 research sites*.

White Rose Research Online URL for this paper:
<http://eprints.whiterose.ac.uk/145096/>

Version: Accepted Version

Article:

Mikkelsen, M., Rimbault, D.L., Barker, P.B. et al. (63 more authors) (2019) Big GABA II: Water-referenced edited MR spectroscopy at 25 research sites. *NeuroImage*, 191. pp. 537-548. ISSN 1053-8119

<https://doi.org/10.1016/j.neuroimage.2019.02.059>

Article available under the terms of the CC-BY-NC-ND licence
(<https://creativecommons.org/licenses/by-nc-nd/4.0/>).

Reuse

This article is distributed under the terms of the Creative Commons Attribution-NonCommercial-NoDerivs (CC BY-NC-ND) licence. This licence only allows you to download this work and share it with others as long as you credit the authors, but you can't change the article in any way or use it commercially. More information and the full terms of the licence here: <https://creativecommons.org/licenses/>

Takedown

If you consider content in White Rose Research Online to be in breach of UK law, please notify us by emailing eprints@whiterose.ac.uk including the URL of the record and the reason for the withdrawal request.



eprints@whiterose.ac.uk
<https://eprints.whiterose.ac.uk/>

Big GABA II: Water-Referenced Edited MR Spectroscopy at 25 Research Sites

Mark Mikkelsen ^{a,b}, Daniel L. Rimbault ^c, Peter B. Barker ^{a,b}, Pallab K. Bhattacharyya ^{d,e}, Maiken K. Brix ^{f,g}, Pieter F. Buur ^h, Kim M. Cecil ⁱ, Kimberly L. Chan ^{a,b,j}, David Y.-T. Chen ^k, Alexander R. Craven ^{l,m}, Koen Cuypers ^{n,o}, Michael Dacko ^p, Niall W. Duncan ^q, Ulrike Dydak ^r, David A. Edmondson ^r, Gabriele Ende ^s, Lars Ersland ^{l,m,t}, Megan A. Forbes ^{u,v}, Fei Gao ^w, Ian Greenhouse ^x, Ashley D. Harris ^y, Naying He ^z, Stefanie Heba ^{aa}, Nigel Hoggard ^{ab}, Tun-Wei Hsu ^{ac}, Jacobus F. A. Jansen ^{ad}, Alayar Kangarlu ^{ae,af}, Thomas Lange ^p, R. Marc Lebel ^{ag}, Yan Li ^z, Chien-Yuan E. Lin ^{ah}, Jy-Kang Liou ^{ac}, Jiing-Feng Lirng ^{ac}, Feng Liu ^{af}, Joanna R. Long ^{ai,aj}, Ruoyun Ma ^{ra,ak}, Celine Maes ⁿ, Marta Moreno-Ortega ^{ae}, Scott O. Murray ^{al}, Sean Noah ^x, Ralph Noeske ^{am}, Michael D. Noseworthy ^{an}, Georg Oeltzschner ^{a,b}, Eric C. Porges ^{u,v}, James J. Prisciandaro ^{ao}, Nicolaas A. J. Puts ^{a,b}, Timothy P. L. Roberts ^{ap}, Markus Sack ^s, Napapon Sailasuta ^{aq,ar}, Muhammad G. Saleh ^{a,b}, Michael-Paul Schallmo ^{al,as}, Nicholas Simard ^{at}, Diederick Stoffers ^h, Stephan P. Swinnen ^{na,au}, Martin Tegenthoff ^{aa}, Peter Truong ^{aq}, Guangbin Wang ^w, Iain D. Wilkinson ^{ab}, Hans-Jörg Wittsack ^{av}, Adam J. Woods ^{u,v}, Hongmin Xu ^z, Fuhua Yan ^z, Chencheng Zhang ^{aw}, Vadim Zipunnikov ^{ax}, Helge J. Zöllner ^{av,ay}, Richard A. E. Edden ^{a,b,*}

^a Russell H. Morgan Department of Radiology and Radiological Science, The Johns Hopkins University School of Medicine, Baltimore, MD, USA

^b F. M. Kirby Research Center for Functional Brain Imaging, Kennedy Krieger Institute, Baltimore, MD, USA

^c Division of Biomedical Engineering, Department of Human Biology, University of Cape Town, Cape Town, South Africa

^d Imaging Institute, Cleveland Clinic Foundation, Cleveland, OH, USA

^e Radiology, Cleveland Clinic Lerner College of Medicine of Case Western Reserve University, Cleveland, OH, USA

^f Department of Radiology, Haukeland University Hospital, Bergen, Norway

^g Department of Clinical Medicine, University of Bergen, Bergen, Norway

^h Spinoza Centre for Neuroimaging, Amsterdam, The Netherlands

- ⁱ Department of Radiology, Cincinnati Children's Hospital Medical Center, Cincinnati, OH, USA
- ^j Department of Biomedical Engineering, The Johns Hopkins University School of Medicine, Baltimore, MD, USA
- ^k Department of Radiology, Taipei Medical University Shuang Ho Hospital, New Taipei City, Taiwan
- ^l Department of Biological and Medical Psychology, University of Bergen, Bergen, Norway
- ^m NORMENT – Norwegian Center for Mental Disorders Research, University of Bergen, Bergen, Norway
- ⁿ Department of Kinesiology, KU Leuven, Leuven, Belgium
- ^o REVAL Rehabilitation Research Center, Hasselt University, Diepenbeek, Belgium
- ^p Department of Radiology, Medical Physics, Medical Center - University of Freiburg, Faculty of Medicine, Freiburg, Germany
- ^q Brain and Consciousness Research Centre, Taipei Medical University, Taipei, Taiwan
- ^r School of Health Sciences, Purdue University, West Lafayette, IN, USA
- ^s Department of Neuroimaging, Central Institute of Mental Health, Mannheim, Germany
- ^t Department of Clinical Engineering, Haukeland University Hospital, Bergen, Norway
- ^u Department of Clinical and Health Psychology, University of Florida, Gainesville, FL, USA
- ^v Center For Cognitive Aging and Memory, McKnight Brain Institute, University of Florida, Gainesville, FL, USA
- ^w Shandong Medical Imaging Research Institute, Shandong University, Jinan, China
- ^x Helen Wills Neuroscience Institute, University of California, Berkeley, Berkeley, CA, USA
- ^y Department of Radiology, University of Calgary, Calgary, AB, Canada
- ^z Department of Radiology, Ruijin Hospital, Shanghai Jiao Tong University School of Medicine, Shanghai, China
- ^{aa} Department of Neurology, BG University Hospital Bergmannsheil, Bochum, Germany
- ^{ab} Academic Unit of Radiology, University of Sheffield, Sheffield, UK
- ^{ac} Department of Radiology, Taipei Veterans General Hospital, National Yang-Ming University School of Medicine, Taipei, Taiwan
- ^{ad} Department of Radiology, Maastricht University Medical Center, Maastricht, The Netherlands
- ^{ae} Department of Psychiatry, Columbia University, New York, NY, USA

- ^{af} New York State Psychiatric Institute, New York, NY, USA
- ^{ag} GE Healthcare, Calgary, AB, Canada
- ^{ah} GE Healthcare, Taipei, Taiwan
- ^{ai} Department of Biochemistry and Molecular Biology, University of Florida, Gainesville, FL, USA
- ^{aj} National High Magnetic Field Laboratory, Gainesville, FL, USA
- ^{ak} Center for Magnetic Resonance Research, Department of Radiology, University of Minnesota, Minneapolis, MN, USA
- ^{al} Department of Psychology, University of Washington, Seattle, WA, USA
- ^{am} GE Healthcare, Berlin, Germany
- ^{an} Department of Electrical and Computer Engineering, McMaster University, Hamilton, ON, Canada
- ^{ao} Department of Psychiatry and Behavioral Sciences, Medical University of South Carolina, Charleston, SC, USA
- ^{ap} *Department of Radiology, Children's Hospital of Philadelphia*, Philadelphia, PA, USA
- ^{aq} Research Imaging Centre, Centre for Addiction and Mental Health, Toronto, ON, Canada
- ^{ar} Department of Psychiatry, University of Toronto, Toronto, ON, Canada
- ^{as} Department of Psychiatry and Behavioral Sciences, University of Minnesota, Minneapolis, MN, USA
- ^{at} School of Biomedical Engineering, McMaster University, Hamilton, ON, Canada
- ^{au} Leuven Research Institute for Neuroscience & Disease (LIND), KU Leuven, Leuven, Belgium
- ^{av} Department of Diagnostic and Interventional Radiology, Medical Faculty, Heinrich-Heine-University, Duesseldorf, Germany
- ^{aw} Department of Functional Neurosurgery, Ruijin Hospital, Shanghai Jiao Tong University School of Medicine, Shanghai, China
- ^{ax} Department of Biostatistics, Johns Hopkins Bloomberg School of Public Health, Baltimore, MD, USA
- ^{ay} Institute of Clinical Neuroscience and Medical Psychology, Medical Faculty, Heinrich-Heine-University, Duesseldorf, Germany

***Corresponding author:** Richard A. E. Edden
Division of Neuroradiology, Park 367H
The Johns Hopkins University School of Medicine
600 N Wolfe St
Baltimore, MD 21287
USA
raee2@jhu.edu

Abstract

Accurate and reliable quantification of brain metabolites measured in vivo using ^1H magnetic resonance spectroscopy (MRS) is a topic of continued interest in the field. Aside from differences in the basic approach to quantification, the quantification of metabolite data acquired at different sites and on different platforms poses an additional methodological challenge. In this study, we analyze spectrally edited γ -aminobutyric acid (GABA) MRS data and quantify GABA levels relative to an internal tissue water reference. Data from 284 volunteers scanned across 25 research sites were collected using standard GABA+ editing. Unsuppressed water acquisitions from the same volume of interest were acquired for signal referencing. Whole-brain T_1 -weighted structural images were acquired and tissue-segmented to determine gray matter, white matter and cerebrospinal fluid voxel tissue fractions. Water-referenced GABA+ measurements were fully corrected for tissue-dependent signal relaxation and water visibility effects. The cohort-wide coefficient of variation was 17%, which was largely driven by vendor-related differences according to a linear mixed-effects analysis. The mean within-site coefficient of variation was 9%. Vendor differences contributed 53% to the total variance in the data, while the remaining variance was attributed to site- (11%) and participant-level (36%) effects. Results from an exploratory analysis suggested that the vendor differences were related to the water signal acquisition. Discounting the observed vendor-specific effects, water-referenced GABA+ measurements exhibit levels of variance similar to creatine-referenced GABA+ measurements. It is concluded that quantification using internal tissue water referencing remains a viable and reliable method for the in vivo quantification of GABA+ levels.

Keywords: Editing; GABA; MEGA-PRESS; MRS; Multi-site study; Quantification; Tissue correction

1. Introduction

In vivo ^1H magnetic resonance spectroscopy (MRS) allows noninvasive measurement of brain metabolite concentrations, but it does so only in a relative manner. Measurements usually rely on an internal reference signal and assumptions about the concentration of the reference compound. Common reference signals include the CH_3 singlets of the metabolites creatine (Cr) and N-acetylaspartate (NAA) and the unsuppressed brain tissue water signal from the same volume. Current opinion in the field suggests that there is no reference signal that is optimal in all applications, and discussion is ongoing about the relative merits of each (Alger, 2010; Mullins et al., 2014).

The theory and empirical feasibility of the absolute quantification of metabolites as measured by MRS is well established (Barker et al., 1993; Christiansen et al., 1993; Danielsen and Henriksen, 1994; Ernst et al., 1993; Hennig et al., 1992; Kreis et al., 1993a; Thulborn and Ackerman, 1983). Later work has further refined and simplified these approaches, particularly with respect to using brain tissue water as an internal concentration reference (Gasparovic et al., 2018, 2006; Gussew et al., 2012; Knight-Scott et al., 2003). The typical procedure for using tissue water as an internal reference is to acquire an unsuppressed water signal using the same MRS acquisition protocol as used for the water-suppressed metabolite acquisition in a voxel co-localized to the volume of interest. With proper assumptions about certain properties of the metabolite and water signals and the concentration of water in the various tissue compartments in the volume of interest, one may infer absolute metabolite concentrations from the acquired metabolite and reference signals. This is supported by the well-characterized properties of MR-visible water in the brain and its high concentration/large signal. On the other hand, using an endogenous metabolite signal, such as Cr, as a reference to derive metabolite ratios avoids the need for a separate water acquisition and may reduce error propagation that arises during more involved signal scaling procedures, but possibly at the expense of lower signal quality. At present, while strong opinions exist on the matter, both metabolite and water referencing have advantages and disadvantages (Jansen et al., 2006), and either approach is defensible. Indeed, the reliability of each approach has been shown to be similar (Bogner et al., 2010; Saleh et al., 2016), although in relatively small studies.

It is important to note that the concentration and relaxation properties of water, Cr and NAA change with disease (Grasso et al., 2002; Huang et al., 2001; Kantarci et al., 2000; Laule et al., 2004; Rackayova et al., 2017), aging (Marjańska et al., 2017; Neeb et al., 2006; Reyncoudt et al., 2012) and development (Kreis et al., 1993b; Tkáč et al., 2003). Phantom replacement, scanning a phantom of a reference compound of known concentration for comparison to in vivo measurements (Buchli and Boesiger, 1993; Duc et al., 1998), can – with careful attention to differences in B_0/B_1 inhomogeneities, amplifier transmitter/receiver gains and RF coil loading factors – also be used to determine in vivo concentrations in absolute units. This method is technically challenging, involving additional experiments before or after the scan session, and is not commonly used given the difficulties of constructing a phantom with electric conductivity similar to human tissue and matching the coil loading factors of the in vivo and phantom samples (Jansen et al., 2006). An alternative approach is the ERETIC (electronic reference to access in vivo concentrations) method (Barantin et al., 1997; Zoelch et al., 2017), which relies on a synthetic RF reference signal. This approach is also challenging and requires specialized hardware. For all its limitations, internal concentration referencing remains the most practicable and widely used approach in in vivo ^1H MRS.

In addition to the nuances of different quantification methodologies, it is clear that systematic differences in acquisition implementation and system hardware will have an impact on quantitative outcomes. This makes comparing MRS measurements collected across different sites and on different platforms non-trivial. If multi-site and multi-platform MRS studies are to be maximally useful, particularly in the era of “big data” (Bearden and Thompson, 2017; Miller et al., 2016; Van Essen et al., 2013), then the systematic effects on measurement variance must be assessed, understood and accounted for. This would then be followed by strategies for standardizing data acquisition, data processing and metabolite quantification methods.

We have recently acquired a large multi-vendor, multi-site dataset, the purpose of which is to study the various sources of variance in γ -aminobutyric acid (GABA) measurements collected by edited MRS. In the first paper describing this dataset (Mikkelsen et al., 2017), quantification was performed relative to the total Cr signal in the edit-OFF spectrum. In this paper, we quantify GABA relative to brain tissue water and account for individual differences in voxel tissue composition. In particular, we seek to determine whether quantification relative to

water increases or decreases total variance (compared to Cr referencing) and discuss the impact of site- and vendor-related differences in structural image segmentation.

2. Methods

A complete description of the acquisition and data processing methodology can be found in our original publication (Mikkelsen et al., 2017). Relevant details for this study, especially regarding quantification and tissue segmentation, are reported below.

2.1. Data collection

Data were acquired at 25 independent research sites, with each site contributing 5–12 datasets collected from consenting adult volunteers (cohort total: 284). Participants at each site were 18–35 years old, approximately 50:50 male/female and had no known neurological or psychiatric illnesses. Site-by-site participant demographics are provided in Table 1 in Mikkelsen et al. (2017). Scanning was conducted in accordance with ethical standards set by the institutional review board (IRB) at each site, including the sharing of anonymized data. Anonymized data files were shared securely with and analyzed by the co-authors at the Johns Hopkins University School of Medicine with local IRB approval.

2.2. Data acquisition

GABA-edited MEGA-PRESS data (Mescher et al., 1998; Rothman et al., 1993) were collected at 3T at each site using a standard scan protocol. The MRI vendor breakdown was: 8 GE; 9 Philips; 8 Siemens. Both standard GABA+-edited and macromolecule-suppressed GABA-edited acquisitions were performed (Edden et al., 2012b). In this paper, only the water-referenced GABA+ data are reported, to avoid redundancy with our prior publication (Mikkelsen et al., 2017). Complete details of the edited MRS acquisitions, including site-to-site idiosyncrasies, can be found in this earlier paper. Briefly, the GABA+ MEGA-PRESS acquisition parameters were: TE/TR = 68/2000 ms; 320 averages; $30 \times 30 \times 30 \text{ mm}^3$ medial parietal lobe voxel (Fig. 1A); ON/OFF editing pulses = 1.9/7.46 ppm; editing pulse duration = 15 ms).

Unsuppressed water signal acquisitions were collected for internal tissue water referencing. For the GE and Philips MEGA-PRESS implementations, the water reference was automatically acquired as part of the water-suppressed metabolite scan. For GE, the reference

was acquired at the end of the suppressed acquisition; 8 or 16 water averages (depending on the specific implementation) were acquired. For Philips, the reference was acquired in an interleaved manner as the water signal was also used for real-time center frequency correction (Edden et al., 2016); a single water average was acquired for every 40 water-suppressed acquisitions (8 averages in total). Acquiring a water reference on the Siemens platform requires running a separate scan. For this, the Siemens MEGA-PRESS WIP was used, where the water suppression RF pulses were turned off but the water suppression gradients and editing pulses were left on (“RF Only” option); 8 or 16 water averages (depending on acquisition parameters) were acquired. The TE/TR of these acquisitions were the same as the water-suppressed acquisitions.

Whole-brain 3D T_1 -weighted structural images were acquired for accurate voxel placement and partial volume tissue correction. Sequences used were fast spoiled gradient-echo imaging (FSPGR; GE) (Low et al., 1993) and magnetization-prepared rapid gradient-echo imaging (MPRAGE; Philips/Siemens) (Mugler and Brookeman, 1990) (see Table 1 for acquisition parameters). Site-standard structural imaging protocols were used, with less effort to standardize acquisitions than the MRS protocols. Imaging data were saved in DICOM (GE and some Siemens sites) or NIfTI format (Philips and some Siemens sites). DICOM files were converted into NIfTI format for voxel segmentation and tissue segmentation purposes (see Section 2.4) using SPM12 (<https://www.fil.ion.ucl.ac.uk/spm/software/spm12/>).

2.3. Data processing

MRS data were processed in Gannet (Edden et al., 2014) using the pipeline described in our earlier report (Mikkelsen et al., 2017). Unsuppressed water acquisitions were processed in the same manner as the water-suppressed acquisitions and averaged. Briefly, processing steps included: frequency-and-phase correction by spectral registration (Near et al., 2015) (water-suppressed data only); 3-Hz exponential line broadening; zero-filling to yield a nominal spectral resolution of 0.061 Hz/point; and fast Fourier transformation into the frequency domain. Quality control and quality metrics were conducted and calculated as before. The linewidth of the water reference was measured as the full-width at half-maximum (FWHM) of the modeled water signal (see Section 2.5). As an independent measure of spectral linewidth, we report NAA FWHM linewidth, measured from the Lorentzian-modeled NAA signal in the OFF spectrum.

2.4. Voxel co-registration and tissue segmentation

MRS voxels were co-registered to each volunteer's structural image using the GannetCoRegister module in Gannet (Harris et al., 2015), which produces binary voxel masks in individual structural space. Structural images were segmented into gray matter (GM), white matter (WM) and cerebrospinal fluid (CSF) probabilistic partial volume maps using the unified tissue segmentation algorithm in SPM12 (Ashburner and Friston, 2005), executed through the GannetSegment module (Harris et al., 2015). Voxel tissue fractions were calculated by multiplying the whole-brain partial volume maps by the corresponding binary voxel mask, summing over the partial volume estimates in the segmented voxel and then dividing by the voxel total.

2.5. Quantification

The 3.0 ppm edited GABA signal was modeled as described in our previous publication (Mikkelsen et al., 2017). The water spectrum was modeled between 3.8 and 5.6 ppm with a Gaussian-Lorentzian function with phase and linear baseline parameters using nonlinear least-squares fitting. GABA+ measurements were quantified in pseudo-absolute concentration units and corrected for partial volume effects (Gasparovic et al., 2006; Harris et al., 2015) based on the following equation:

$$C_G = \frac{I_G}{I_W} \cdot \frac{H_W}{H_G} \cdot \frac{MM}{\kappa} \cdot \left(\frac{\sum_i^{\text{GM,WM,CSF}} C_{W,i} \exp\left(-\frac{TE_W}{T_{2W,i}}\right) \left[1 - \exp\left(-\frac{TR_W}{T_{1W,i}}\right)\right] f_i}{\exp\left(-\frac{TE_G}{T_{2G}}\right) \left[1 - \exp\left(-\frac{TR_G}{T_{1G}}\right)\right]} \right) \cdot \left[\frac{\mu_{\text{GM}} + \alpha \mu_{\text{WM}}}{(f_{\text{GM}} + \alpha f_{\text{WM}})(\mu_{\text{GM}} + \mu_{\text{WM}})} \right] \quad (1)$$

where C_G is the GABA+ concentration in institutional units (i.u.); I_G and I_W are the GABA+ and water signal integrals, respectively; H_W and H_G are the number of ^1H protons that give rise to the water and 3.0 ppm GABA signals (both 2), respectively; MM is a correction factor for the contribution of the co-edited macromolecule signal in the GABA+ signal, assumed to be 0.45; and κ is the editing efficiency, assumed to be 0.5. TE_G , TE_W , TR_G and TR_W are the echo and relaxation times of the GABA-edited and water acquisitions, respectively. $T_{1W,i}$ is the longitudinal relaxation time of water in GM (assumed to be 1331 ms), WM (assumed to be 832 ms) (Wansapura et al., 1999) or CSF (assumed to be 3817 ms) (Lu et al., 2005); $T_{2W,i}$ is the transverse relaxation time of water in GM (assumed to be 110 ms), WM (assumed to be 79.2 ms) (Wansapura et al., 1999) or CSF (assumed to be 503 ms) (Piechnik et al., 2009). T_{1G} and T_{2G} are the longitudinal and transverse relaxation times of GABA, assumed to be 1310 and 88 ms, respectively (Edden et al., 2012a; Puts et al., 2013). $C_{W,i}$ is the concentration of MR-visible water

in GM (assumed to be 43.30 mol/kg), WM (assumed to be 36.08 mol/kg) or CSF (assumed to be 53.84 mol/kg) (Ernst et al., 1993; Gasparovic et al., 2006); f_i is the volume fraction of GM, WM or CSF in the MRS voxel. α is a correction factor that accounts for the relative differences in the intrinsic concentration of GABA in WM and GM (Harris et al., 2015), assumed to be 0.5 (Mikkelsen et al., 2016); μ_{GM} and μ_{WM} are the average GM and WM voxel volume fractions averaged at the site level, which normalize the α -corrected GABA+ values to the site-mean f_{GM} (Harris et al., 2015).

Fit quality for the water peak model (the fit error) was assessed by normalizing the standard deviation (SD) of the model fit residuals to the amplitude of the modeled signal (Edden et al., 2014). This metric, the degree to which the measured signal cannot accurately be modeled as a Gaussian-Lorentzian, captures eddy current artifacts and some aspects of sub-optimal shimming.

To examine whether systematic effects on the variance of the GABA+ data were attributed to the water acquisition, we also quantified water-referenced Cr measurements. The 3.0 ppm Cr signal in the OFF spectrum was modeled as described in our previous publication. The longitudinal and transverse relaxation times of Cr were assumed to be 1350 and 154 ms, respectively (Mlynárik et al., 2001); α was assumed to be 0.5 (Doyle et al., 1995; Wang and Li, 1998). MM and κ were not applied. Finally, we examined the degree of association between participants' water-referenced, tissue-corrected GABA+ values and their previously quantified GABA+/Cr values as reported in Mikkelsen et al. (2017). It should be noted that these measurements are not independent (the GABA+ integral being a common factor) and, therefore, a strong correlation was expected.

2.6. Exploratory analysis

The results revealed systematically higher water-referenced GABA+ measurements from the Siemens sites as compared to the GE and Philips measurements (see Section 3). This level of variation was not apparent in the Cr-referenced GABA+ measurements that we previously reported (Mikkelsen et al., 2017). To reconcile this, we conducted an unplanned exploratory analysis in which the Siemens GABA+ measurements were referenced to a water signal acquired by a separate unsuppressed short-TE PRESS acquisition that was collected alongside the MEGA-PRESS data (data to be reported on in an upcoming publication). This acquisition was acquired

at TE/TR = 35/2000 ms from a voxel in the same location as the MEGA-PRESS acquisition. Concentrations were quantified according to Eq. (1) without additional correction for any possible amplifier gain differences between the PRESS and MEGA-PRESS acquisitions.

2.7. Statistical analysis

Linear mixed-effects models were fit to the water-referenced GABA+ data in R (version 3.5.1; R Core Team) using the lme4 package (Bates et al., 2015) and maximum likelihood for parameter estimation. An unconditional model (Eq. (1) in Mikkelsen et al., 2017) was fit to calculate variance partition coefficients (VPCs) to estimate the proportion of total variance attributed to vendor-, site- and participant-related effects. Secondary, conditional linear mixed-effects models (Eq. (5) in Mikkelsen et al., 2017) were also fit to the data to assess the impact of NAA linewidth, f_{GM} , age and sex, and to test the association with GABA+/Cr measurements. Goodness-of-fit was calculated as a log-likelihood statistic. Significance testing was performed using chi-square likelihood ratio tests, which were bootstrapped 2,000 times using parametric bootstrapping (Halekoh and Højsgaard, 2014). Effects were tested in the following order: vendor and site; NAA linewidth and f_{GM} ; age and sex. If an effect was significant, the relevant variable was retained in the next model; if not, it was removed. Unconditional linear mixed-effects models were also fit to the voxel tissue fractions to test for site and vendor effects. Post-hoc pairwise comparisons were corrected for multiple comparisons using the Holm-Bonferroni method (Holm, 1979). A p-value less than 0.05 was considered significant.

3. Results

Data from seven volunteers were removed from further analysis following quality control of the MRS data (largely due to excessive lipid contamination). One further dataset was removed because the unusually small water reference signal indicated an acquisition error. Vendor-mean GABA+-edited difference spectra are shown in Fig. 1B.

Fig. 2 shows the GABA+ values arranged by site and by vendor. Mean \pm 1 SD GABA+ measurements were 2.45 ± 0.30 i.u. for GE, 2.46 ± 0.27 i.u. for Philips and 3.15 ± 0.36 i.u. for Siemens. Siemens values were on average 29% higher than the GE ($p_{\text{Holm}} < 0.001$) and Philips ($p_{\text{Holm}} < 0.001$) values. The cohort-wide average was 2.67 ± 0.45 i.u. Coefficients of variation (CVs) were 12.4%, 10.8% and 11.3% for GE, Philips and Siemens, and 16.7% across all sites

and vendors. The mean within-site CV was 9.4%. GM, WM and CSF fractions are displayed in Fig. 3. Across the cohort, the average (and CV of) f_{GM} , f_{WM} and f_{CSF} was 0.59 ± 0.04 (6.9%), 0.28 ± 0.04 (14.0%) and 0.13 ± 0.05 (36.7%), respectively. Values of GABA+, f_{GM} , f_{WM} and f_{CSF} for each site are listed in Table 2.

Water fit errors, water linewidths and Cr measurements are displayed in Fig. 4, with site- and vendor-averaged values given in Table 2. On average, fit errors were small, and lower for Siemens (0.38%) compared to GE (0.56%) and Philips (0.56%). Water linewidths were similar across the vendors, with Philips (9.01 ± 0.62 Hz) and Siemens (9.04 ± 0.57 Hz) showing slightly smaller linewidths compared to GE (9.37 ± 0.84 Hz). Average water-referenced Cr measurements were 10.78 ± 0.90 i.u. for GE, 11.95 ± 1.17 i.u. for Philips and 14.73 ± 1.19 i.u. for Siemens.

3.1. Linear mixed-effects analyses

The unconditional linear mixed-effects model showed that vendor and site effects contributed significantly to the total amount of variance in the data: $\chi^2(1) = 27.62$, $p_{boot} < 0.001$ and $\chi^2(1) = 30.40$, $p_{boot} < 0.001$, respectively. Based on the calculated VPCs, 52.9% of the variance was accounted for by vendor-level differences, while 11.2% was accounted for by site-level differences. The remaining proportion of variance (35.9%) was attributed to individual differences in participants.

The voxel tissue fractions exhibited significant site-related effects for f_{GM} [$\chi^2(1) = 56.33$, $p_{boot} = 0.001$], f_{WM} [$\chi^2(1) = 46.77$, $p_{boot} < 0.001$] and f_{CSF} [$\chi^2(1) = 47.22$, $p_{boot} < 0.001$], but only f_{WM} showed an additional vendor-related effect [$\chi^2(1) = 4.08$, $p_{boot} = 0.01$]. Corresponding VPCs for f_{GM} were: vendor = negligible; site = 31.4%; participant = 68.6%. For f_{WM} these were: vendor = 12.8%; site = 24.9%; participant = 62.3%. For f_{CSF} these were: vendor = 1.8%; site = 28.5%; participant = 69.7%. Pairwise comparisons showed that, at the vendor level, the Siemens f_{WM} values were significantly higher than the GE ($p_{holm} = 0.001$) and Philips ($p_{holm} = 0.003$) values.

Based on the conditional linear mixed-effects analyses, GABA+ levels were not significantly impacted by the effects of NAA linewidth [$\chi^2(5) = 4.37$, $p_{boot} = 0.50$]. GABA+ levels did, however, show a relationship with f_{GM} [$\chi^2(5) = 10.14$, $p_{boot} = 0.02$]. To examine the effectiveness of the metabolite tissue correction (i.e., the α -correction term in Eq. (1)), the by-site and cohort-wide effects of f_{GM} on the tissue-water-corrected GABA+ data before and after α -

correction are displayed in Fig. 5. The pre-corrected data show a strong association with f_{GM} ($R^2 = 0.18$) that is reduced after α -correction ($R^2 = 0.08$), a 50% decrease in the variance shared with f_{GM} . There were no significant effects of age [$\chi^2(5) = 1.77$, $p_{boot} = 0.88$] or sex [$\chi^2(5) = 0.88$, $p_{boot} = 0.97$] on the data. As shown in Fig. 6, the water-referenced GABA+ measurements were strongly related to the GABA+/Cr measurements, as expected [$\chi^2(5) = 253.86$, $p_{boot} < 0.001$].

3.2. Exploratory analysis

Using the Siemens short-TE water reference brought down the Siemens GABA+ values to an average of 2.68 ± 0.32 i.u. (a 15% reduction), reducing the discrepancy with the other vendors to 9% (boxplots plotted in Fig. S1). Corresponding VPCs were: vendor = 10.9%; site = 24.4%; participant = 64.6%, with vendor and site effects remaining significant: $\chi^2(1) = 3.43$, $p_{boot} = 0.02$ and $\chi^2(1) = 33.01$, $p_{boot} < 0.001$, respectively. The short-TE-referenced Siemens Cr measurements were also reduced on average (by 14%, to 12.60 ± 1.49 i.u.) compared to the initial analysis, again closer to the GE and Philips Cr measurements (Fig. S2).

4. Discussion

In this second paper on a large multi-vendor, multi-site GABA-edited MRS dataset, we have shown that water-referenced GABA+ measurements, including tissue correction based on variously acquired T_1 -weighted structural images, can be applied across sites and vendors with relatively low levels of variance. Water-referenced quantification shows very similar levels of performance to Cr referencing, as reported previously (Mikkelsen et al., 2017), with the notable exception of an additional vendor-related effect.

One objective of this study was to compare quantitative outcomes of water and Cr referencing. Within site, water- and Cr-referenced GABA+ measurements show very similar levels of variance (mean within-site CV: 9.4% vs. 9.5%, respectively). Levels of site-related variance are also similar (mean within-vendor CV: 11.5% vs. 11.3%, respectively). The major difference between the water- and Cr-referenced results was the systematic effect of vendor in the water-referenced data.

It is not clear why the GABA+ values from the Siemens data were substantially larger than the estimates from the other two vendors. This substantial vendor-related difference was not observed in the Cr-referenced data reported previously (Mikkelsen et al., 2017). Higher GABA+

values indicate a lower-than-expected water signal. Referencing to a short-TE PRESS water acquisition attenuated the discrepancy somewhat, suggesting that the Siemens MEGA-PRESS WIP water reference signal is most likely at issue. It is notable that the water fit errors were somewhat lower in the Siemens data, suggesting that the water signal is closer to a Gaussian-Lorentzian lineshape than the other vendors. It is worth mentioning that the data analyzed undergo differing degrees of preprocessing (e.g., downsampling from the analog-to-digital converter sampling rate to the specified acquisition rate), with potentially different dynamic range performance – the water reference signal is ~10,000 times larger than the GABA signal and acquired with the same receiver gains. At this stage, it has not been possible to isolate the cause of this result.

Aside from this vendor effect, it was clear that the variation in the water-referenced GABA+ measurements was quite similar to the GABA+/Cr measurements. This suggests that the reliability of these two referencing strategies is comparable, consistent with previous (smaller) studies (Bogner et al., 2010; Saleh et al., 2016). This is perhaps surprising as several additional corrections were performed to obtain the water-referenced values, which introduces more sources of error into the quantification.

Quantification in this study used a best-practice approach, whereby the water reference signal was corrected for partial volume effects and relaxation. It has been shown that failing to account for these effects will lead to quantification errors (Gasparovic et al., 2018). These errors can be particularly pronounced at longer TEs (Gasparovic et al., 2006) or when there is large variability in tissue compartment fractions across cohorts (Harris et al., 2015; Mato Abad et al., 2014; Mikkelsen et al., 2016; Tal et al., 2012). The relatively low level of variance in the present dataset suggests that incorporating image-based voxel segmentation into the quantification routine did not add significant variance into the data.

Nonetheless, subtle differences in quantification and tissue correction methodologies can have important consequences on reported results. For instance, the linear relationship between GABA+ levels and age, seen when applying a simple CSF tissue correction, is not observed when applying fuller α -correction to remove the dependency of GABA+ levels on tissue composition (Maes et al., 2018; Porges et al., 2017). Additionally, the units of measurement of water-referenced metabolite concentrations, and the information content of the values, will depend on the quantification approach used. Metabolite concentrations have been reported in

molar, molal and institutional units (Gasparovic et al., 2018; Jansen et al., 2006; Knight-Scott et al., 2003; Kreis et al., 1993a). Interpretation of stated concentrations, and particularly comparisons across studies, can be challenging. In this study, we report our measurements in institutional units. This was in part because the α -correction applied to the tissue-water-corrected measurements effectively normalized the site-level values to the amount of GABA+ that theoretically would have been observed would the signal have been detected in a voxel composed of a fraction of GM and WM equal to the average of fractional GM and WM of the site-specific cohort. This does not prevent the values from being compared across studies, however; it simply demonstrates that the values presented here may differ from those presented elsewhere as a result of the quantification approach that was used.

Not every possible source of variance was captured in the statistical analysis. One source of error, for instance, was the diversity of the T_1 -weighted structural imaging protocols. Differences in imaging preparation and readout will result in heterogeneity in T_1 -weighted contrast and image signal-to-noise ratio, which might in turn lead to variable segmentation outcomes. In our data, there were small but significant site-to-site differences in voxel segmentation. There is an extensive literature on the successes and limitations of image segmentation (Clark et al., 2006; Eggert et al., 2012; Klauschen et al., 2009), and while segmentation algorithms aim to be robust against the effects of imaging parameters, segmentation remains a challenging undertaking. At this stage, it is unclear to what degree error from segmentation inaccuracies propagates into metabolite quantification. The substantial tissue differences in water T_2 , particularly given the medium TE of the water acquisitions (68 ms), and in GABA and MR-visible water concentrations, suggest that accurate segmentation is important for reproducible water-referenced quantification.

In summary, we quantified GABA+ levels using brain tissue water as an internal concentration reference across 25 sites and observed low levels of within-site variance. This level of variability is similar to that seen for GABA+ measurements quantified relative to Cr. Thus, the choice of reference signal for MRS quantification is not determined by inherent differences in performance, but rather by study-specific expectations of reference signal stability (e.g., between-group differences in clinical populations). Indeed, given the concern that observed effects might be driven by changes in the reference signal, it is often helpful to quantify both

water- and metabolite-referenced measurements. That said, we conclude that water-referenced measurements of GABA+ are sufficiently reliable to be applied in multi-site studies.

Appendix

The data presented in this work has been made available on the NITRC portal in the “Big GABA” project repository (https://www.nitrc.org/projects/big_gaba/) and is distributed freely under a non-commercial Creative Commons license. Community members are encouraged to make use of this resource for developing and optimizing new MRS methods. This data resource can also serve as a normative dataset against which clinical data may be compared or for quality assurance purposes.

Acknowledgments

This work was supported by NIH grants R01 EB016089, R01 EB023963 and P41 EB015909. Data collection was supported by the Shandong Provincial Key Research and Development Plan of China (2016ZDJS07A16) and the National Natural Science Foundation of China for Young Scholars (no. 81601479). IDW [and NH](#) thanks Mrs. J. Bigley of the University of Sheffield MRI Unit for her assistance with data acquisition, [The Wellcome Trust and the NIHR-Sheffield Biomedical Research Centre](#). JJP was supported by NIAAA grant K23 AA020842. MPS was supported by NIH grant F32 EY025121. ECP was supported by NIAAA grant K01 AA025306 and the University of Florida, Center for Cognitive Aging and Memory and McKnight Brain Research Foundation. NAJP receives salary support from NIH grant R00 MH107719. The authors acknowledge implementation contributions from a number of employees of Siemens Medical Solutions, including Dr. Keith Heberlein and Dr. Sinyeob Ahn, to the Siemens WIP sequences, which are shared with several research sites under sequence-specific agreements.

References

- Alger, J.R., 2010. Quantitative Proton Magnetic Resonance Spectroscopy and Spectroscopic Imaging of the Brain. *Top. Magn. Reson. Imaging* 21, 115–128. doi:10.1097/RMR.0b013e31821e568f
- Ashburner, J., Friston, K.J., 2005. Unified segmentation. *Neuroimage* 26, 839–851. doi:10.1016/j.neuroimage.2005.02.018
- Barantin, L., Pape, A. Le, Akoka, S., 1997. A new method for absolute quantitation MRS metabolites. *Magn. Reson. Med.* 38, 179–182. doi:10.1002/mrm.1910380203
- Barker, P.B., Soher, B.J., Blackband, S.J., Chatham, J.C., Mathews, V.P., Bryan, R.N., 1993. Quantitation of proton NMR spectra of the human brain using tissue water as an internal concentration reference. *NMR Biomed.* 6, 89–94. doi:10.1002/nbm.1940060114
- Bates, D., Mächler, M., Bolker, B.M., Walker, S.C., 2015. Fitting linear mixed-effects models using lme4. *J. Stat. Softw.* 67. doi:10.18637/jss.v067.i01
- Bearden, C.E., Thompson, P.M., 2017. Emerging Global Initiatives in Neurogenetics: The Enhancing Neuroimaging Genetics through Meta-analysis (ENIGMA) Consortium. *Neuron* 94, 232–236. doi:10.1016/j.neuron.2017.03.033
- Bogner, W., Gruber, S., Doelken, M., Stadlbauer, A., Ganslandt, O., Boettcher, U., Trattnig, S., Doerfler, A., Stefan, H., Hammen, T., 2010. In vivo quantification of intracerebral GABA by single-voxel 1H-MRS—How reproducible are the results? *Eur. J. Radiol.* 73, 526–531. doi:10.1016/j.ejrad.2009.01.014
- Buchli, R., Boesiger, P., 1993. Comparison of methods for the determination of absolute metabolite concentrations in human muscles by 31P MRS. *Magn. Reson. Med.* 30, 552–558. doi:10.1002/mrm.1910300505
- Christiansen, P., Henriksen, O., Stubgaard, M., Gideon, P., Larsson, H.B.W., 1993. In vivo quantification of brain metabolites by 1H-MRS using water as an internal standard. *Magn. Reson. Imaging* 11, 107–118. doi:10.1016/0730-725X(93)90418-D
- Clark, K.A., Woods, R.P., Rottenberg, D.A., Toga, A.W., Mazziotta, J.C., 2006. Impact of acquisition protocols and processing streams on tissue segmentation of T1 weighted MR

- images. *Neuroimage* 29, 185–202. doi:10.1016/j.neuroimage.2005.07.035
- Danielsen, E.R., Henriksen, O., 1994. Absolute quantitative proton NMR spectroscopy based on the amplitude of the local water suppression pulse. Quantification of brain water and metabolites. *NMR Biomed.* 7, 311–318. doi:10.1002/nbm.1940070704
- Doyle, T.J., Bedell, B.J., Narayana, P.A., 1995. Relative Concentrations of Proton MR Visible Neurochemicals in Gray and White Matter in Human Brain. *Magn. Reson. Med.* 33, 755–759. doi:10.1002/mrm.1910330603
- Duc, C.O., Weber, O.M., Trabesinger, A.H., Meier, D., Boesiger, P., 1998. Quantitative ¹H MRS of the human brain in vivo based on the stimulation phantom calibration strategy. *Magn. Reson. Med.* 39, 491–6. doi:10.1002/mrm.1910390320
- Edden, R.A.E., Intrapromkul, J., Zhu, H., Cheng, Y., Barker, P.B., 2012a. Measuring T2 in vivo with J-difference editing: Application to GABA at 3 Tesla. *J. Magn. Reson. Imaging* 35, 229–234. doi:10.1002/jmri.22865
- Edden, R.A.E., Oeltzschner, G., Harris, A.D., Puts, N.A.J., Chan, K.L., Boer, V.O., Schär, M., Barker, P.B., 2016. Prospective frequency correction for macromolecule-suppressed GABA editing at 3T. *J. Magn. Reson. Imaging* 44, 1474–1482. doi:10.1002/jmri.25304
- Edden, R.A.E., Puts, N.A.J., Barker, P.B., 2012b. Macromolecule-suppressed GABA-edited magnetic resonance spectroscopy at 3T. *Magn. Reson. Med.* 68, 657–661. doi:10.1002/mrm.24391
- Edden, R.A.E., Puts, N.A.J., Harris, A.D., Barker, P.B., Evans, C.J., 2014. Gannet: A batch-processing tool for the quantitative analysis of gamma-aminobutyric acid-edited MR spectroscopy spectra. *J. Magn. Reson. Imaging* 40, 1445–1452. doi:10.1002/jmri.24478
- Eggert, L.D., Sommer, J., Jansen, A., Kircher, T., Konrad, C., 2012. Accuracy and Reliability of Automated Gray Matter Segmentation Pathways on Real and Simulated Structural Magnetic Resonance Images of the Human Brain. *PLoS One* 7, e45081. doi:10.1371/journal.pone.0045081
- Ernst, T., Kreis, R., Ross, B.D., 1993. Absolute quantitation of water and metabolites in the human brain. I. Compartments and water. *J. Magn. Reson. Ser. B* 102, 1–8. doi:10.1006/jmrb.1993.1055

- Gasparovic, C., Chen, H., Mullins, P.G., 2018. Errors in 1H-MRS estimates of brain metabolite concentrations caused by failing to take into account tissue-specific signal relaxation. *NMR Biomed.* 31, e3914. doi:10.1002/nbm.3914
- Gasparovic, C., Song, T., Devier, D., Bockholt, H.J., Caprihan, A., Mullins, P.G., Posse, S., Jung, R.E., Morrison, L.A., 2006. Use of tissue water as a concentration reference for proton spectroscopic imaging. *Magn. Reson. Med.* 55, 1219–1226. doi:10.1002/mrm.20901
- Grasso, G., Alafaci, C., Passalacqua, M., Morabito, A., Buemi, M., Salpietro, F.M., Tomasello, F., 2002. Assessment of Human Brain Water Content by Cerebral Bioelectrical Impedance Analysis: A New Technique and Its Application to Cerebral Pathological Conditions. *Neurosurgery* 50, 1064–1074. doi:10.1097/00006123-200205000-00023
- Gussew, A., Erdtel, M., Hiepe, P., Rzanny, R., Reichenbach, J.R., 2012. Absolute quantitation of brain metabolites with respect to heterogeneous tissue compositions in 1H-MR spectroscopic volumes. *Magn. Reson. Mater. Physics, Biol. Med.* 25, 321–333. doi:10.1007/s10334-012-0305-z
- Halekoh, U., Højsgaard, S., 2014. A Kenward-Roger approximation and parametric bootstrap methods for tests in linear mixed models - The R package pbrtest. *J. Stat. Softw.* 59, 1–32. doi:10.18637/jss.v059.i09
- Harris, A.D., Puts, N.A.J., Edden, R.A.E., 2015. Tissue correction for GABA-edited MRS: Considerations of voxel composition, tissue segmentation, and tissue relaxations. *J. Magn. Reson. Imaging* 42, 1431–1440. doi:10.1002/jmri.24903
- Hennig, J., Pfister, H., Ernst, T., Ott, D., 1992. Direct absolute quantification of metabolites in the human brain within vivo localized proton spectroscopy. *NMR Biomed.* 5, 193–199. doi:10.1002/nbm.1940050406
- Holm, S., 1979. A simple sequentially rejective multiple test procedure. *Scand. J. Stat.* 6, 65–70.
- Huang, W., Alexander, G.E., Chang, L., Shetty, H.U., Krasuski, J.S., Rapoport, S.I., Schapiro, M.B., 2001. Brain metabolite concentration and dementia severity in Alzheimer's disease: A 1H MRS study. *Neurology* 57, 626–632. doi:10.1212/WNL.57.4.626
- Jansen, J.F.A., Backes, W.H., Nicolay, K., Kooi, M.E., 2006. 1H MR Spectroscopy of the Brain: Absolute Quantification of Metabolites. *Radiology* 240, 318–332.

doi:10.1148/radiol.2402050314

- Kantarci, K., Jack, C.R., Xu, Y.C., Campeau, N.G., O'Brien, P.C., Smith, G.E., Ivnik, R.J., Boeve, B.F., Kokmen, E., Tangalos, E.G., Petersen, R.C., 2000. Regional metabolic patterns in mild cognitive impairment and Alzheimer's disease: A 1H MRS study. *Neurology* 55, 210–217. doi:10.1212/WNL.55.2.210
- Klauschen, F., Goldman, A., Barra, V., Meyer-Lindenberg, A., Lundervold, A., 2009. Evaluation of automated brain MR image segmentation and volumetry methods. *Hum. Brain Mapp.* 30, 1310–1327. doi:10.1002/hbm.20599
- Knight-Scott, J., Haley, A.P., Rossmiller, S.R., Farace, E., Mai, V.M., Christopher, J.M., Manning, C. a., Simnad, V.I., Siragy, H.M., 2003. Molality as a unit of measure for expressing 1H MRS brain metabolite concentrations in vivo. *Magn. Reson. Imaging* 21, 787–797. doi:10.1016/S0730-725X(03)00179-6
- Kreis, R., Ernst, T., Ross, B.D., 1993a. Absolute quantitation of water and metabolites in the human brain. II. Metabolite concentrations. *J. Magn. Reson. Ser. B* 102, 9–19. doi:10.1006/jmrb.1993.1056
- Kreis, R., Ernst, T., Ross, B.D., 1993b. Development of the human brain: In vivo quantification of metabolite and water content with proton magnetic resonance spectroscopy. *Magn. Reson. Med.* 30, 424–437. doi:10.1002/mrm.1910300405
- Laule, C., Vavasour, I.M., Moore, G.R.W., Oger, J., Li, D.K.B., Paty, D.W., MacKay, A.L., 2004. Water content and myelin water fraction in multiple sclerosis. A T2 relaxation study. *J. Neurol.* 251, 284–93. doi:10.1007/s00415-004-0306-6
- Low, R.N., Francis, I.R., Herfkens, R.J., Jeffrey, R.B., Glazer, G.M., Foo, T.K., Shimakawa, A., Pelc, N.J., 1993. Fast multiplanar spoiled gradient-recalled imaging of the liver: pulse sequence optimization and comparison with spin-echo MR imaging. *Am. J. Roentgenol.* 160, 501–509. doi:10.2214/ajr.160.3.8381572
- Lu, H., Nagae-Poetscher, L.M., Golay, X., Lin, D., Pomper, M., van Zijl, P.C.M., 2005. Routine clinical brain MRI sequences for use at 3.0 Tesla. *J. Magn. Reson. Imaging* 22, 13–22. doi:10.1002/jmri.20356
- Maes, C., Hermans, L., Pauwels, L., Chalavi, S., Leunissen, I., Levin, O., Cuypers, K., Peeters, R.,

- Sunaert, S., Mantini, D., Puts, N.A.J., Edden, R.A.E., Swinnen, S.P., 2018. Age-related differences in GABA levels are driven by bulk tissue changes. *Hum. Brain Mapp.* 39, 3652–3662. doi:10.1002/hbm.24201
- Marjańska, M., McCarten, J.R., Hodges, J., Hemmy, L.S., Grant, A., Deelchand, D.K., Terpstra, M., 2017. Region-specific aging of the human brain as evidenced by neurochemical profiles measured noninvasively in the posterior cingulate cortex and the occipital lobe using 1 H magnetic resonance spectroscopy at 7 T. *Neuroscience* 354, 168–177. doi:10.1016/j.neuroscience.2017.04.035
- Mato Abad, V., Quirós, A., García-Álvarez, R., Loureiro, J.P., Álvarez-Linera, J., Frank, A., Hernández-Tamames, J.A., 2014. The Partial Volume Effect in the Quantification of 1H Magnetic Resonance Spectroscopy in Alzheimer’s Disease and Aging. *J. Alzheimer’s Dis.* 42, 801–811. doi:10.3233/JAD-140582
- Mescher, M., Merkle, H., Kirsch, J., Garwood, M., Gruetter, R., 1998. Simultaneous in vivo spectral editing and water suppression. *NMR Biomed.* 11, 266–272. doi:10.1002/(SICI)1099-1492(199810)11:6<266::AID-NBM530>3.0.CO;2-J
- Mikkelsen, M., Barker, P.B., Bhattacharyya, P.K., Brix, M.K., Buur, P.F., Cecil, K.M., Chan, K.L., Chen, D.Y.-T., Craven, A.R., Cuyper, K., Dacko, M., Duncan, N.W., Dydak, U., Edmondson, D.A., Ende, G., Ersland, L., Gao, F., Greenhouse, I., Harris, A.D., He, N., Heba, S., Hoggard, N., Hsu, T., Jansen, J.F.A., Kangarlu, A., Lange, T., Lebel, R.M., Li, Y., Lin, C.E., Liou, J., Lirng, J.-F., Liu, F., Ma, R., Maes, C., Moreno-Ortega, M., Murray, S.O., Noah, S., Noeske, R., Noseworthy, M.D., Oeltzschner, G., Prisciandaro, J.J., Puts, N.A.J., Roberts, T.P.L., Sack, M., Sailasuta, N., Saleh, M.G., Schallmo, M., Simard, N., Swinnen, S.P., Tegenthoff, M., Truong, P., Wang, G., Wilkinson, I.D., Wittsack, H.-J., Xu, H., Yan, F., Zhang, C., Zipunnikov, V., Zöllner, H.J., Edden, R.A.E., 2017. Big GABA: Edited MR spectroscopy at 24 research sites. *Neuroimage* 159, 32–45. doi:10.1016/j.neuroimage.2017.07.021
- Mikkelsen, M., Singh, K.D., Brealy, J.A., Linden, D.E.J., Evans, C.J., 2016. Quantification of γ -aminobutyric acid (GABA) in 1H MRS volumes composed heterogeneously of grey and white matter. *NMR Biomed.* 29, 1644–1655. doi:10.1002/nbm.3622
- Miller, K.L., Alfaro-Almagro, F., Bangerter, N.K., Thomas, D.L., Yacoub, E., Xu, J., Bartsch,

- A.J., Jbabdi, S., Sotiropoulos, S.N., Andersson, J.L.R., Griffanti, L., Douaud, G., Okell, T.W., Weale, P., Dragonu, I., Garratt, S., Hudson, S., Collins, R., Jenkinson, M., Matthews, P.M., Smith, S.M., 2016. Multimodal population brain imaging in the UK Biobank prospective epidemiological study. *Nat. Neurosci.* 19, 1523–1536. doi:10.1038/nn.4393
- Mlynárik, V., Gruber, S., Moser, E., 2001. Proton T1 and T2 relaxation times of human brain metabolites at 3 Tesla. *NMR Biomed.* 14, 325–331. doi:10.1002/nbm.713
- Mugler, J.P., Brookeman, J.R., 1990. Three-dimensional magnetization-prepared rapid gradient-echo imaging (3D MP RAGE). *Magn. Reson. Med.* 15, 152–157. doi:10.1002/mrm.1910150117
- Mullins, P.G., McGonigle, D.J., O’Gorman, R.L., Puts, N.A.J., Vidyasagar, R., Evans, C.J., Cardiff Symposium on MRS of GABA, Edden, R.A.E., 2014. Current practice in the use of MEGA-PRESS spectroscopy for the detection of GABA. *Neuroimage* 86, 43–52. doi:10.1016/j.neuroimage.2012.12.004
- Near, J., Edden, R., Evans, C.J., Paquin, R., Harris, A., Jezzard, P., 2015. Frequency and phase drift correction of magnetic resonance spectroscopy data by spectral registration in the time domain. *Magn. Reson. Med.* 73, 44–50. doi:10.1002/mrm.25094
- Neeb, H., Zilles, K., Shah, N.J., 2006. Fully-automated detection of cerebral water content changes: Study of age- and gender-related H2O patterns with quantitative MRI. *Neuroimage* 29, 910–922. doi:10.1016/j.neuroimage.2005.08.062
- Piechnik, S.K., Evans, J., Bary, L.H., Wise, R.G., Jezzard, P., 2009. Functional changes in CSF volume estimated using measurement of water T2 relaxation. *Magn. Reson. Med.* 61, 579–586. doi:10.1002/mrm.21897
- Porges, E.C., Woods, A.J., Lamb, D.G., Williamson, J.B., Cohen, R.A., Edden, R.A.E., Harris, A.D., 2017. Impact of tissue correction strategy on GABA-edited MRS findings. *Neuroimage* 162, 249–256. doi:10.1016/j.neuroimage.2017.08.073
- Puts, N.A.J., Barker, P.B., Edden, R.A.E., 2013. Measuring the longitudinal relaxation time of GABA in vivo at 3 Tesla. *J. Magn. Reson. Imaging* 37, 999–1003. doi:10.1002/jmri.23817
- R Core Team, 2018. R: A Language and Environment for Statistical Computing. R Foundation for Statistical Computing, Vienna, Austria. <https://www.R-project.org/>.

- Rackayova, V., Cudalbu, C., Pouwels, P.J.W., Braissant, O., 2017. Creatine in the central nervous system: From magnetic resonance spectroscopy to creatine deficiencies. *Anal. Biochem.* 529, 144–157. doi:10.1016/j.ab.2016.11.007
- Reyngoudt, H., Claeys, T., Vlerick, L., Verleden, S., Acou, M., Deblaere, K., De Deene, Y., Audenaert, K., Goethals, I., Achten, E., 2012. Age-related differences in metabolites in the posterior cingulate cortex and hippocampus of normal ageing brain: A ¹H-MRS study. *Eur. J. Radiol.* 81, e223–e231. doi:10.1016/j.ejrad.2011.01.106
- Rothman, D.L., Petroff, O.A., Behar, K.L., Mattson, R.H., 1993. Localized ¹H NMR measurements of gamma-aminobutyric acid in human brain in vivo. *Proc. Natl. Acad. Sci. U. S. A.* 90, 5662–6.
- Saleh, M.G., Near, J., Alhamud, A., Robertson, F., van der Kouwe, A.J.W., Meintjes, E.M., 2016. Reproducibility of macromolecule suppressed GABA measurement using motion and shim navigated MEGA-SPECIAL with LCMoDel, jMRUI and GANNET. *Magn. Reson. Mater. Physics, Biol. Med.* 29, 863–874. doi:10.1007/s10334-016-0578-8
- Tal, A., Kirov, I.I., Grossman, R.I., Gonen, O., 2012. The role of gray and white matter segmentation in quantitative proton MR spectroscopic imaging. *NMR Biomed.* 25, 1392–1400. doi:10.1002/nbm.2812
- Thulborn, K.R., Ackerman, J.J., 1983. Absolute molar concentrations by NMR in inhomogeneous B1. A scheme for analysis of in vivo metabolites. *J. Magn. Reson.* 55, 357–371. doi:10.1016/0022-2364(83)90118-X
- Tkáč, I., Rao, R., Georgieff, M.K., Gruetter, R., 2003. Developmental and regional changes in the neurochemical profile of the rat brain determined by in vivo ¹H NMR spectroscopy. *Magn. Reson. Med.* 50, 24–32. doi:10.1002/mrm.10497
- Van Essen, D.C., Smith, S.M., Barch, D.M., Behrens, T.E.J., Yacoub, E., Ugurbil, K., 2013. The WU-Minn Human Connectome Project: An overview. *Neuroimage* 80, 62–79. doi:10.1016/j.neuroimage.2013.05.041
- Wang, Y., Li, S.-J., 1998. Differentiation of metabolic concentrations between gray matter and white matter of human brain by in vivo ¹H magnetic resonance spectroscopy. *Magn. Reson. Med.* 39, 28–33. doi:10.1002/mrm.1910390107

- Wansapura, J.P., Holland, S.K., Dunn, R.S., Ball, W.S., 1999. NMR relaxation times in the human brain at 3.0 Tesla. *J. Magn. Reson. Imaging* 9, 531–538. doi:10.1002/(SICI)1522-2586(199904)9:4<531::AID-JMRI4>3.0.CO;2-L
- Zoelch, N., Hock, A., Heinzer-Schweizer, S., Avdievitch, N., Henning, A., 2017. Accurate determination of brain metabolite concentrations using ERETIC as external reference. *NMR Biomed.* 30, e3731. doi:10.1002/nbm.3731

Fig. 1. (A) Representative MRS voxel placement on a T₁-weighted structural image and probabilistic partial volume voxel maps following tissue segmentation for one participant. Corresponding tissue fractions of gray matter (GM), white matter (WM) and cerebrospinal fluid (CSF) are shown. (B) Vendor-mean GABA⁺-edited difference spectra. The gray patches represent ± 1 standard deviation. The associated sample sizes are shown in parentheses.

Fig. 2. Water-referenced GABA⁺ measurements fully corrected for partial volume effects, displayed by site and by vendor. The boxes shaded with lighter colors represent ± 1 standard deviation and the darker boxes represent the 95% confidence interval. The solid white lines denote the mean, while the dashed white lines denote the median. Sites are colored by vendor (GE sites in green, Philips sites in orange, Siemens sites in blue).

Fig. 3. Gray matter (GM), white matter (WM) and cerebrospinal fluid (CSF) voxel tissue fractions, displayed by site and by vendor. GM = gray fill; WM = white fill; CSF = black fill. The red lines denote the mean. Sites are colored by vendor (GE sites with a green background, Philips sites with an orange background, Siemens sites with a blue background).

Fig. 4. Quality metrics and water-referenced Cr measurements, displayed by site and by vendor. (A) water fit error; (B) water linewidth; (C) Cr measurements fully corrected for partial volume effects. The boxes shaded with lighter colors represent ± 1 standard deviation and the darker boxes represent the 95% confidence interval. The solid white lines denote the mean, while the dashed white lines denote the median. Sites are colored by vendor (GE sites in green, Philips sites in orange, Siemens sites in blue).

Fig. 5. Scatterplots displaying tissue-water-corrected GABA⁺ measurements as a function of gray matter voxel tissue fraction (f_{GM}) (A) before and (B) after α -correction to account for intrinsic differences in gray and white matter GABA. Individual measurements are color-coded by vendor (GE in green, Philips in orange, Siemens in blue). The black regression lines show the relationship between f_{GM} and water-referenced GABA⁺ over the entire dataset. Additional color-coded regression lines are shown for each site. R^2 values (i.e., effect sizes) are also displayed.

Fig. 6. Scatterplot illustrating the relationship between water-referenced GABA+ measurements and GABA+/Cr ratios. Individual measurements are color-coded by vendor (GE in green, Philips in orange, Siemens in blue). The black regression line shows the relationship between GABA+/Cr and water-referenced GABA+ over the entire dataset. Additional color-coded regression lines are shown for each site. The R^2 value (i.e., the effect size) is also displayed.

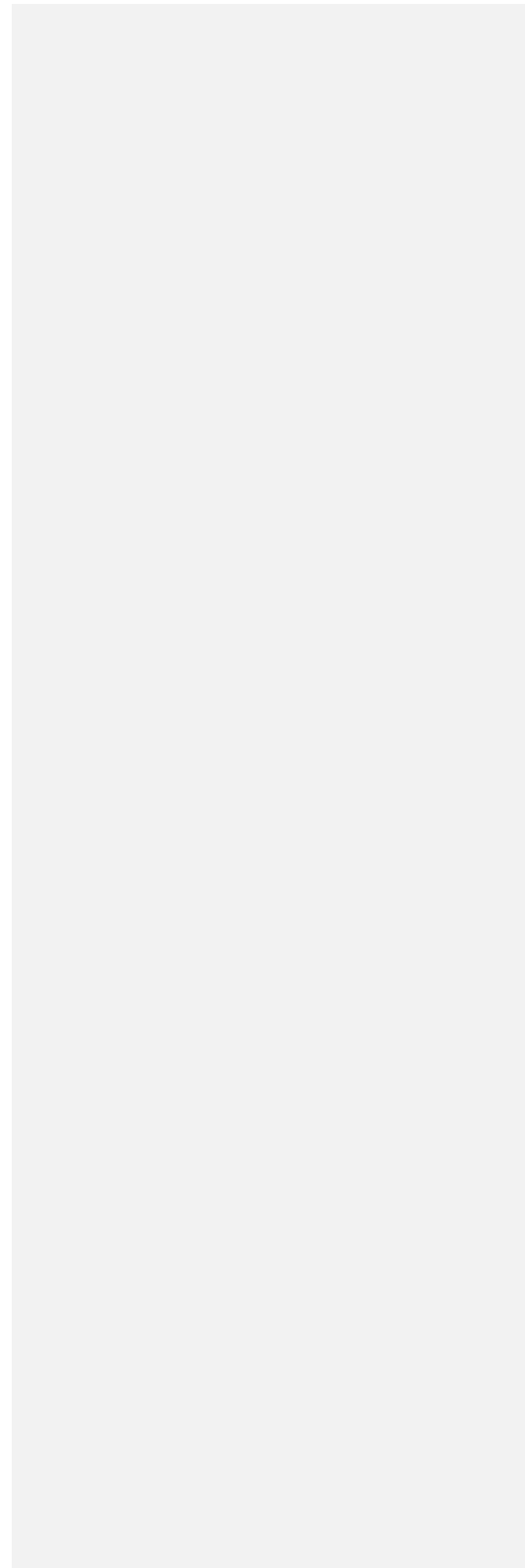


Table 1. Hardware and acquisition parameters used to collect 3D T₁-weighted structural images at each site.

Site ID	Tx/Rx hardware	Voxel resolution (mm ³)	TE/TI/TR (ms)	Scan time (m:ss)	Flip angle (deg)	Slices	FOV (mm ²)	Matrix size	Acceleration (factor)
G1	Body coil/32-ch head coil	0.94 × 0.94 × 1	2.68/600/7.42	4:07	10	226	256 × 256	256 × 256	ASSET (2)
G2	Body coil/8-ch head coil	0.9 × 0.9 × 1	2.73/650/6.24	2:54	8	180	256 × 256	256 × 256	ARC (2)
G3	Body coil/32-ch head coil	1 × 1 × 1	2.6/500/6.4	4:37	11	180	256 × 256	256 × 256	ASSET (2)
G4	Body coil/8-ch head coil	1 × 1 × 1	2.98/450/6.89	9:35	12	192	256 × 256	256 × 256	None
G5	Body coil/32-ch head coil	0.5 × 0.5 × 0.8	2.1/450/7.09	5:39	12	232	256 × 256	512 × 512	None
G6	Body coil/8-ch head coil	1 × 1 × 2	2.66/400/6.24	6:22	12	124	240 × 240	240 × 240	None
G7	Body coil/8-ch head coil	1 × 1 × 1	3.2/450/8.2	4:30	12	176	256 × 256	256 × 256	ARC (2)
G8	Body coil/8-ch head coil	1 × 1 × 1	4.17/450/10.19	5:27	12	180	256 × 256	256 × 256	ARC (2)
P1	Body coil/32-ch head coil	1 × 1 × 1	3.1/865/6.9	7:10	8	204	256 × 256	256 × 256	SENSE (2)
P2	Body coil/32-ch head coil	1 × 1 × 1	3.1/865/6.9	7:10	8	204	256 × 256	256 × 256	SENSE (2)
P3	Body coil/32-ch head coil	1 × 1 × 1	3.1/865/6.9	7:10	8	204	256 × 256	256 × 256	SENSE (2)
P4	Body coil/32-ch head coil	1 × 1 × 1	3.1/865/6.9	7:10	8	204	256 × 256	256 × 256	SENSE (2)
P5	Body coil/32-ch head coil	1 × 1 × 1	3.1/865/6.9	7:10	8	170	256 × 256	256 × 256	SENSE (2)
P6	Body coil/8-ch head coil	1 × 1 × 1	3.1/865/6.9	7:10	8	204	256 × 256	256 × 256	SENSE (2)
P7	Body coil/32-ch head coil	1 × 1 × 1	3.1/865/6.9	7:10	8	204	256 × 256	256 × 256	SENSE (2)
P8	Body coil/32-ch head coil	1 × 1 × 1	3.1/865/6.9	7:10	8	204	256 × 256	256 × 256	SENSE (2)
P9	Body coil/32-ch head coil	1 × 1 × 1	3.1/865/6.9	7:10	8	176	256 × 256	256 × 256	SENSE (2)
S1	Body coil/32-ch head coil	1 × 1 × 1	2.52/900/1900	4:18	9	176	250 × 250	256 × 256	GRAPPA (2)
S2	Body coil/32-ch head coil	1 × 1 × 1	2.85/1050/1900	5:43	9	176	256 × 256	256 × 256	GRAPPA (2)
S3	Body coil/20-ch head/neck coil	1 × 1 × 1	1.77/900/1900	4:05	8	160	256 × 256	128 × 256	GRAPPA (2)
S4	Body coil/64-ch head coil	1 × 1 × 1	4.11/1000/2000	3:36	12	160	256 × 256	256 × 256	GRAPPA (2)
S5	Body coil/12-ch head coil	1 × 1 × 1	4.6/900/1950	4:01	9	176	192 × 256	192 × 256	GRAPPA (2)
S6	Body coil/32-ch head coil	1 × 1 × 1	2.26/900/1900	4:26	9	192	256 × 256	256 × 256	GRAPPA (2)
S7	Body coil/32-ch head coil	1 × 1 × 1	3.03/900/2300	5:21	9	192	256 × 256	256 × 256	GRAPPA (2)
S8	Body coil/64-ch head coil	1 × 1 × 1	3.02/900/1900	4:01	9	160	256 × 256	256 × 256	GRAPPA (2)

Table 2. Quantification, tissue fractions and water data quality metrics, displayed by site and by vendor (shown as mean \pm 1 standard deviation).

Site ID	GABA+ (i.u.)	Cr (i.u.)	f _{GM}	f _{WM}	f _{CSF}	Water fit error (%)	Water linewidth (Hz)
G1	2.47 \pm 0.13	11.69 \pm 1.00	0.60 \pm 0.05	0.26 \pm 0.04	0.14 \pm 0.03	0.95 \pm 0.09	9.43 \pm 0.48
G2	2.72 \pm 0.19	11.19 \pm 0.61	0.56 \pm 0.02	0.29 \pm 0.03	0.15 \pm 0.03	0.57 \pm 0.11	9.98 \pm 0.73
G3	2.15 \pm 0.19	10.16 \pm 0.69	0.60 \pm 0.03	0.29 \pm 0.02	0.11 \pm 0.03	0.43 \pm 0.09	9.46 \pm 0.76
G4	2.45 \pm 0.28	10.54 \pm 0.52	0.60 \pm 0.03	0.28 \pm 0.02	0.12 \pm 0.04	0.42 \pm 0.06	9.34 \pm 0.40
G5	2.20 \pm 0.16	10.33 \pm 0.41	0.65 \pm 0.05	0.26 \pm 0.01	0.09 \pm 0.04	0.55 \pm 0.11	9.79 \pm 0.63
G6	2.36 \pm 0.42	9.65 \pm 0.76	0.54 \pm 0.04	0.32 \pm 0.02	0.15 \pm 0.04	0.65 \pm 0.07	9.80 \pm 0.92
G7	2.56 \pm 0.28	11.28 \pm 0.55	0.57 \pm 0.05	0.23 \pm 0.02	0.19 \pm 0.06	0.47 \pm 0.11	8.72 \pm 0.88
G8	2.56 \pm 0.28	11.10 \pm 0.49	0.57 \pm 0.03	0.23 \pm 0.05	0.21 \pm 0.05	0.41 \pm 0.09	8.40 \pm 0.42
All GE	2.45 \pm 0.30	10.78 \pm 0.90	0.58 \pm 0.05	0.27 \pm 0.04	0.15 \pm 0.05	0.56 \pm 0.19	9.37 \pm 0.84
P1	2.44 \pm 0.28	11.46 \pm 0.78	0.60 \pm 0.03	0.27 \pm 0.04	0.13 \pm 0.04	0.47 \pm 0.07	8.78 \pm 0.53
P2	2.34 \pm 0.19	11.55 \pm 0.71	0.56 \pm 0.03	0.29 \pm 0.02	0.15 \pm 0.04	0.43 \pm 0.07	8.74 \pm 0.40
P3	2.42 \pm 0.18	11.24 \pm 0.94	0.58 \pm 0.02	0.29 \pm 0.03	0.13 \pm 0.03	0.84 \pm 0.11	9.02 \pm 0.43
P4	2.58 \pm 0.42	11.86 \pm 0.56	0.59 \pm 0.02	0.26 \pm 0.02	0.15 \pm 0.03	0.32 \pm 0.06	8.78 \pm 0.38
P5	2.24 \pm 0.18	11.32 \pm 0.75	0.63 \pm 0.03	0.27 \pm 0.02	0.11 \pm 0.03	0.75 \pm 0.08	9.06 \pm 0.24
P6	2.64 \pm 0.20	13.19 \pm 1.19	0.57 \pm 0.02	0.25 \pm 0.03	0.18 \pm 0.05	0.67 \pm 0.17	8.71 \pm 0.53
P7	2.30 \pm 0.16	11.88 \pm 0.47	0.63 \pm 0.03	0.27 \pm 0.03	0.10 \pm 0.03	0.69 \pm 0.11	10.21 \pm 0.62
P8	2.66 \pm 0.23	13.84 \pm 0.54	0.61 \pm 0.04	0.28 \pm 0.03	0.11 \pm 0.04	0.40 \pm 0.04	9.03 \pm 0.29
P9	2.45 \pm 0.17	11.13 \pm 0.93	0.59 \pm 0.02	0.28 \pm 0.04	0.12 \pm 0.03	0.50 \pm 0.06	8.77 \pm 0.31
All Philips	2.46 \pm 0.27	11.95 \pm 1.17	0.59 \pm 0.04	0.27 \pm 0.03	0.13 \pm 0.04	0.56 \pm 0.19	9.01 \pm 0.62
S1	3.06 \pm 0.17	14.76 \pm 0.84	0.57 \pm 0.03	0.30 \pm 0.03	0.12 \pm 0.05	0.39 \pm 0.08	9.40 \pm 0.72
S2	3.47 \pm 0.29	17.24 \pm 0.28	0.55 \pm 0.02	0.33 \pm 0.02	0.12 \pm 0.03	0.38 \pm 0.03	9.22 \pm 0.36
S3	2.83 \pm 0.30	14.86 \pm 0.98	0.56 \pm 0.03	0.33 \pm 0.04	0.11 \pm 0.04	0.30 \pm 0.06	8.63 \pm 0.39
S4	3.16 \pm 0.33	14.05 \pm 0.57	0.61 \pm 0.03	0.29 \pm 0.02	0.10 \pm 0.04	0.33 \pm 0.05	8.81 \pm 0.31
S5	3.28 \pm 0.53	14.45 \pm 1.60	0.59 \pm 0.05	0.31 \pm 0.04	0.10 \pm 0.07	0.42 \pm 0.11	9.45 \pm 0.92
S6	3.01 \pm 0.11	14.57 \pm 0.42	0.59 \pm 0.04	0.30 \pm 0.03	0.11 \pm 0.03	0.44 \pm 0.08	9.12 \pm 0.28
S7	3.27 \pm 0.25	13.88 \pm 0.96	0.58 \pm 0.03	0.28 \pm 0.03	0.14 \pm 0.04	0.46 \pm 0.08	8.98 \pm 0.39
S8	3.31 \pm 0.38	15.52 \pm 0.61	0.58 \pm 0.03	0.29 \pm 0.03	0.13 \pm 0.02	0.33 \pm 0.07	8.84 \pm 0.36
All Siemens	3.15 \pm 0.37	14.73 \pm 1.19	0.58 \pm 0.04	0.30 \pm 0.04	0.12 \pm 0.04	0.38 \pm 0.10	9.04 \pm 0.57
Overall	2.67 \pm 0.45	12.42 \pm 1.94	0.59 \pm 0.04	0.28 \pm 0.04	0.13 \pm 0.05	0.51 \pm 0.19	9.14 \pm 0.70